CONF-8504152--9

7/16/85

BNL 36877
OG 850

BNL--36877

DE85 017841

A DETECTOR FOR DIMUONS PRODUCED IN THE RELATIVISTIC HEAVY ION COLLIDER

* S. Aronson, BNL
G. Igo, UCLA
B. Pope, MSU
* A. Shor, BNL
G. Young, ORNL

* Co-convenors

SEP 17 1985

MASTER

Presented at Workshop on Experiments for
Relativistic Heavy Ion Collider
BNL, Upton, NY, April 15-19, 1985

DISCLAIMER

A DETECTOR FOR DIMUONS PRODUCED IN THE RELATIVISTIC HEAVY ION COLLIDER

*S. Aronson, BNL
G. Igo, UCLA
B. Pope, MSU
*A. Shor, BNL
G. Young, ORNL

*Co-convenors

The use of dimuons as a probe of the quark-gluon plasma is explored. Expected rates and backgrounds in the range of dimuon masses from 0.5 to 4.0 GeV/c^2 are presented. A conceptual design is developed for a detector with sufficient resolution and background rejection to observe dimuons in high multiplicity collisions expected at RHIC. Machine requirements and a cost estimate for the detector are also presented.

I. INTRODUCTION

The Dimuon Working Group was a small but dedicated group of experimentalists with diverse backgrounds and experience. Expertise in heavy ion and particle physics, including colliding beam experiments and dilepton experiments was present. It was clear that in some kinematical regions the dimuon experiment was not only doable but one of the most doable experiments in the relativistic heavy ion collision environment. The question was, is it doable in a kinematical region of interest in the context of the quark-gluon plasma?

We sought the counsel of a number of theorists at the Workshop. With their guidance as to what dimuon masses and transverse momenta are interesting, we developed the spectrometer presented here. This is a rough version which we believe could form the basis of a real physics proposal for RHIC.

In sections II and III we present a general overview, addressing the usefulness of dimuons as a probe of the plasma and the basic principles of dimuon detection. Sections IV, V and VI go into these subjects in more

*This research supported by the U.S. Department of Energy under Contract No. DE-AC02-76CH00016.

detail, discussing dimuon rates in hadronic production, the problem of dimuon detection in plasma events, and reviewing models of dimuon signals from the plasma. In section VII we present the details of the detector design concept and discuss its acceptance, resolution and associated "fake μ" backgrounds. Section VIII is a rough but reasonably complete cost estimate; section IX is a list of topics for further work necessary to convert this idea into a defensible proposal. Section X summarizes the presentation.

Following the summary is a collection of appendices which give somewhat more detail on specific aspects of the work. The topics are listed below:

1. Absorber instrumentation (Appendix 1)
2. Absorber Monte Carlo (Appendix 2)
3. Toroid design considerations (Appendices 3,4)
4. Machine physics questions (Appendix 5)

II. DIMUONS AS PROBE OF THE PLASMA

Dimuons - Elegant Probe of the QGP

Dimuons serve as a very elegant tool for probing the quark-gluon plasma. The advantages and simplifications inherent in the study of dimuons originate from theoretical as well as from experimental considerations.

Dimuons Penetrate Plasma - Hadrons Don't

Dimuons are produced in the plasma when a quark and anti-quark annihilate to form a virtual photon. Since they interact only electro-weakly, the dimuons, once produced, can penetrate the plasma without any further interaction (see Fig. 1). The dimuons, therefore, carry information from a hot environment which is dense with quarks and anti-quarks. Hadrons, on the other hand, do not exist in the plasma but materialize only at the surface of the plasma. The hadrons, at best, can only provide information about the environment in which the plasma proceeds to hadronize at the critical temperature T_c. This situation is actually worse because almost all hadrons will interact further during the expanding hadronic phase and will only reflect the conditions during the hadronic freezeout.

It is also hoped that the dimuon production rate over some mass interval will be enhanced if a QGP is formed. This expectation is born out in several theoretical treatments.[1]

Dimuons Penetrate Detectors - Hadrons Don't

Experimentally, the measurement of dimuons in high energy nuclear collisions provides great simplification over the measurement of hadrons. For central collisions of Au-Au at $\sqrt{s}/n$ = 200 GeV, over 4,000 hadrons will be produced. To track these hadrons, or even some fraction of them, would pose a great and possibly insurmountable experimental challenge. Another option would be to absorb all the hadrons with a sensitive hadronic calorimeter which would provide information on $d^2E/dyd\phi$. Muons of sufficient energy would not be absorbed, but would emerge from the calorimeter into conventional tracking detectors (see Fig. 2). The measurement of the invariant mass of a $\mu^+\mu^-$ along with the rapidity and P_T of the pair, can easily be obtained. The dimuons can in turn be correlated with rapidity fluctuations or with events with a large E_T.

III. PRINCIPLES OF DETECTION AND KINEMATIC LIMITS

Muon detection and identification is straightforward, although difficult in the present case. Muons are detected by their survival after sufficient material to absorb electrons, photons and hadrons. Hadrons can fake muons by decaying into muons before interaction, or by "punch-through", wherein a low energy charged particle from the hadronic shower exits the absorber. The difficulty in the case of relativistic heavy ion collisions arises from the very large multiplicity of charged hadrons and from the requirement to detect quite low energy muons.

In order to reduce the hadron-induced background the absorber needs to be as close as possible to the interaction point (to reduce decays) and sufficiently thick to contain hadronic showers. For a given absorber thickness muons below a certain energy will be ranged out or so badly multiple-scattered as to be unusable in any measurement of the dimuon spectrum. The resulting lower limit on the energy of useful muons translates into lower limits on the mass or transverse momentum of muon pairs; the kinematic quantity of interest is the so-called transverse mass:

$$m_T = (m_{\mu\mu}^2 + p_T^2)^{1/2}$$

The transverse mass limits attainable with the present detector are discussed in Section VII below.

After surviving the absorber, the muon candidates must be analyzed in order to be reconstructed into pairs. This is done by magnetic momentum analysis. Charged particle tracking chambers are arrayed in a magnetic field and are used to determine both the direction and momentum of the particles leaving the absorber.

A passive absorber destroys all information about the event other than that contained in the muon candidates (at least in that part of the solid angle subtended by the absorber). One can (and presumably desires to) measure other properties of events containing dimuons; this can be done by suitably instrumenting the absorber itself. By making the absorber an active calorimeter and segmenting it into "towers," one can measure the energy flow $d^2E/dyd\phi$ and trigger on events with large transverse energy, transverse energy imbalance, jets, large fluctuations in the rapidity distribution of energy, anomalous ratios of electromagnetic and hadronic energy, etc.

Below in Section VII, after a discussion of expected muon rates and of plasma event characteristics we return to a more specific detector configuration and present its properties and limitations.

IV. DIMUON PRODUCTION - HADRONIC BACKGROUND

The mass of the dimuons determines the space-time scale of the hadronic interaction which is being probed. Three distinct production mechanisms are identified with three different mass intervals. The best understood is Drell-Yan which is applicable to pair masses above 4-5 GeV. This mechanism is due to hard quark-antiquark annihilation at the initial stage of the hadronic collisions, and provides information on the structure functions of the initial quarks in the colliding hadrons. The second mass range involves the annihilation of quarks and antiquarks produced at later stages of the hadronic interaction and is relevant to the interval from M_ρ to about 4 GeV.[2] A good fit of dimuons over this mass interval has been obtained by Shuryak assuming a thermal distribution of quarks and antiquarks.[3] This mass range is presumably the most relevant for a thermal quark-gluon plasma. The third range of dimuon masses involves masses below that of the $\rho(M_\rho \approx 770$ MeV). In this range $\pi^+\pi^-$ annihilation plays an important role and may account for the anomalous lepton pairs observed at low masses.[4] In addition,

there are dimuons produced by the electromagnetic decay of vector mesons, i.e., ρ, ω, ϕ and J/ψ.

A calculation for hadronic dimuon production in Au and Au collisions at $\sqrt{s}$ = 200 GeV/n is shown in Figure 3. The calculation includes the following parameterization

(i) $M^5 \frac{d\sigma}{dmdy}\Big|_{y=0} = 3 \times 10^{-4} (1 - \sqrt{\tau})^7$ for the continuum where $\sqrt{\tau} = \frac{M}{\sqrt{s}}$ (Ref.5)

(ii) $F(x_f) = (1 - x_f)^{3.5}$ where $x_f = (p/p_{max})_{c.m.}$ (Ref.5)

(iii) $\frac{d\sigma}{dp_T^2} = N e^{-6E_T}$ where $E_T = \sqrt{m^2+p_T^2} - m$ and $N = \frac{6^2}{2(6m + 1)}$ (Ref.5)

(iv) A^{α}: $\alpha = .67 + .11m$, $1 < m < 3$ (Ref.6)
$\alpha = 1$, $m > 3$

(v) ρ_0 : $\sigma_{inc} = (.38\ \ell n^2 s - 2.1)$mb (Ref.7)
ϕ : $\sigma_{inc} = (.27\ \ell ns - .86)$mb (Ref.8)

(vi) Assumptions:
a) $\sigma_{central\ collision} = 0.01\ \sigma_{reaction}$
b) $\sigma_{AA} = \sigma_{pp} A^{2\alpha}$.

Both of these assumptions are arbitrary and need to be studied in more detail.

V. Dimuon Detection in Plasma Events

There are three issues to be investigated in determining the feasibility of dimuon detection in relativistic heavy ion collisions: coverage, sensitivity and resolution.

The issue of coverage (i.e. what fraction of the solid angle should be subtended by the detector) is influenced by luminosity and expected event rates as well as by kinematics. From the point of view of rate it makes

sense to cover as much as possible of the solid angle where good sensitivity can be achieved. This rather weak dictum stems from our uncertainties about the dimuon rate from the QGP. However, the kinematics issue also points to wide coverage so we turn our attention to this point. As discussed in Section VI below, one wants to detect dimuons over a reasonably broad range of masses or transverse momenta: between about 4 GeV, above which ordinary hadronic dimuon production will dominate, and about 0.5 GeV to cover the resonances.

Events at the high end of the range can be studied relatively easy at low rapidities (θ near 90°); here the relatively energetic muons can penetrate an absorber thick enough to suppress the "punch-through" background (see Table I in Section VII). In the special case of high dimuon mass at small y and small p_T (i.e., back-to-back muons) the multiple scattering error on the muon angles contributes negligibly to mass resolution.

For small values of mass or p_T (i.e. soft muons or small opening angles) it is only possible to detect dimuons at large rapidities (small θ), where the boosted laboratory momenta are sufficient to survive the absorber. Here however, angular resolution is much more important ($m_{\mu\mu}^2 \propto E_1 E_2 \theta^2$). As will be seen in Section VII below we have adopted the strategy of a longer, lower density absorber to get a lower multiple scattering limit on resolution (see Table II in Section VII). Since the mean multiple scattering angle $\theta_{ms} \propto \sqrt{L/\chi_0}$ then the material with the largest ratio of radiation length to absorption length will give the least multiple scattering for a given number of absorption lengths. For example, uranium, which we choose for compactness in most of the solid angle, has $\chi_0/\lambda_0 = 0.03$, while aluminum gives 0.23 and beryllium gives 0.87.

The problems of sensitivity and resolution are most severe in the forward region. This is so for the reasons given above, plus the fact that the density and energy of background particles is greatest here. One is looking for narrow features in the dimuon mass spectrum in this region as well (i.e.- resonances) putting a high premium on resolution.

VI. PHYSICS PRIORITIES-THEORETICAL INPUT

Review of Models for Dimuon Signals from Plasma

Given the limitations in making complete and accurate measurements, the physics objectives for dimuon study need to be established. A number of theoreticians were present at the RHIC workshop, several of whom addressed our working group and assisted us in establishing the physics priorities.

A presentation by R. Hwa at the workshop proved to be very informative. Hwa argued that the dimuons of interest are thermally produced by $q\bar{q}$ annihilation in a plasma which is formed at an initial temperature T_i, cools while expanding, and hadronizes at the deconfinement temperature T_c. The relevant dimuon parameter to measure is m_T with the optimal quark phase contribution at $T_c < m_T/5.5 < T_i$. With $200 < T < 500$ MeV, the interesting transverse masses are at $1 < m_T < 3$ GeV. Hwa speculates that the contribution from the plasma in this mass interval may be an order of magnitude larger than for hadronic production. He suggested that the dimuon spectrum $d^2\sigma/dm^2dy$ can be correlated with dN_π/dy (or alternatively with dE/dy). He warned us about contaminations from other sources of $\mu^+\mu^-$ for $m_T < 1$ GeV.

A. Goldhaber visited our working group during the Workshop. He suggested that it may be more fruitful initially to look at higher pair masses in the Drell-Yan region since this region is well understood. Deviations from systematics observed in pp and pA reactions, for example the dependence on A, may prove to be interesting. We could then work our way down to lower masses where the physics is less clear.

During the discussions it was mentioned that significant deviations from Drell-Yan already exist for pp collisions. Some of these deviations are explained by QCD corrections. Two examples are the K-factor and transverse momentum dependence, both of which can be accounted for by soft gluon exponentiation terms.[9] It would be interesting to study how the environment of the plasma would affect these known corrections to Drell-Yan.

We are left with a situation in which we would want to measure both the low transverse masses in the range $1 < m_T < 3$ GeV and also larger masses in the Drell-Yan region. Unfortunately, we can only measure low masses for the

intermediate rapidity region and high masses accurately for low rapidities. In this context, the discussion our working group had with L. McLerran proved to be extremely helpful. McLerran suggested that the plasma would be a plateau elongated in rapidity and its properties would be independent of the position on the plateau as long as we remain outside of the baryon rich region (see Fig. 4). It is therefore not necessary to measure a given value of M_T at all values of y. Our experimental limitation of low masses at $2 < y < 3$ and higher masses at $|y| < 2$ is not a serious limitation. This also means that we will need top energies so that we can open up the baryon free plateau.

In addition to measuring dimuons from the continuum, a measurement of dimuons from hadronic resonances may prove to be quite interesting. The ρ_0 would experience "melting" in a hot nuclear environment - its mass would downshift and its width would be broadened.[10] This signal would be a precursor to the restoration of chiral symmetry. Production of the ϕ-meson, composed of a strange and anti-strange quark, would be enhanced if a plasma is formed.[11] The ϕ rescatters very little in the hadronic phase and would carry information on the conditions at the deconfinement temperature T_c.[12] The same arguments would be applicable to the production of the J/ψ if sufficient equilibration is reached in the plasma.[13]

We also had discussions with P. Siemens at the later stages of the Workshop. He suggested that it would be interesting to measure low mass pairs in the continuum with $2m_\pi < m < m_\rho$ at large p_T. Presumably, at large P_T anomalous effects that are present in hadronic production disappear. We would require the ability to resolve the ρ.

The theoretical input we received over the course of the Workshop gave us confidence that we can construct a spectrometer that would do a very satisfactory job. We do want to measure dimuons at low pair masses and at high masses. However, we do not need to measure a given mass over all the rapidity plateau. A spectrometer that can measure all values of m somewhere in the interval $0 < |y| < 3$ would be very adequate. We need to resolve the resonances because they are interesting signals and so that they will not

distort the continuum. We also will need top energies (50-100 GeV/n) where the baryon free plateau is ± 3 units of rapidity.

VII. DESCRIPTION OF THE DIMUON DETECTOR AND ITS PROPERTIES

Figure 5 shows a plan view of the detector from the crossing point to one end of the insertion. Although the principles of muon detection discussed in Section III above are adhered to throughout, different components are used for the central ($|y| < 2$) and forward ($2 < y < 3$) regions. This is because of the desire to measure dimuons in the lowest possible transverse mass in the forward regions, as discussed in Sections IV, V, and VI above. The detector can be symmetrical about the crossing point but for what follows we assume the forward region is instrumented as shown on one side only. We discuss the details of the detector in the two regions below.

A. Central Detector

The absorber is a cylinder with radius = 75 cm and length = ± 100 cm. The density (13 gm/cc) and absorption length (15 cm) are typical of an instrumented uranium calorimeter. The inner surface of the absorber is 1 cm from the beam line. The authors benefited from discussions on the properties of the insertion with S.Y. Lee. Further details are presented in Appendix 5. The muon range cutoff varies from about 1.6 GeV at y = 0 to about 2.8 GeV at y = ± 1.1. The instrumentation of the absorber for energy flow triggering and measurement is discussed in Appendix 1.

A simulation program was written to compute the raw singles rate of fake muon candidtates surviving the absorber. A description of the program is found in Appendix 2. Table I gives a summary of the calculations.

Following the absorber is a set of magnetized iron toroids interleaved with planes of proportional drift tubes for measuring the muon's direction and momentum. Each toroid provides a kick equivalent to ≈90 MeV/c transverse momentum; there are 7 toroids in the range $|y| < 1$ increasing to 10 in the $1 < |y| < 2$ range. The toroids are described in more detail in Appendix 3.

B. Forward Spectrometer

For $2 < y < 3$ ($15° > \theta > 5°$) the attempt is made to reduce multiple scattering and thereby to measure lower transverse mass dimuons. This is accomplished by using a lower Z absorber (larger ratio of radiation length to

absorption length) and an air-core magnet system. Figure 5 shows an aluminum absorber of the same number of absorption lengths as the neighboring central absorber. Lower Z with reasonable density would be even better. Proportional drift tube planes and air-core toroids (paired with opposite fields for better acceptance) provide the forward magnetic analysis. The toroids are described in Appendix 4. Following the magnetic spectrometer is an additional two absorption lengths of material preceded and followed by scintillation hodoscopes for triggering and time-of-flight measurements. The angular region $\theta < 5^\circ$ is left open; the high momentum hadrons in this region would punch through any reasonable absorber and produce large background rates in the forward spectrometer. At a later time additional apparatus capable of studying the baryon rich region ($|y| > 3$) might be placed on the side opposite the forward spectrometer.

Table II summarizes the features of the forward as well as the central part of the detector. Figure 6 is a plot of the mass resolution of the detector as a function of rapidity.

The expected rate of dimuons from hadronic processes can be estimated from Fig. 3b and the design luminosity. For gold on gold ($\sigma \approx 6$ barn, of which $\approx 1\%$ is central collisions) at $L = 3 \times 10^{26}$ cm^{-2}sec^{-1} one expects ≈ 20 central collisions/sec. From the figure one can estimate the dimuon rate to be $\approx 10^{-3}$/central collision, yielding 70 real dimuons from conventional sources per hour of running. Given the raw singles rate for fake μ's in Table I (≈ 60/event over all rapidities covered) one can achieve comparable fake dimuon rates with a 400-to-1 rejection of such fakes by the muon spectrometers outside the absorber. This may be achievable at the trigger level, requiring that they are single tracks pointing back to the source within multiple scattering resolution.

TABLE I

Fake "μ" Singles rates for the Absorber Described in Section VII ($r = 75$ cm, $\ell = \pm 100$ cm, $\lambda_{abs} = 15$ cm)

	$\|y\|<0.5$	$0.5<\|y\|<1.0$	$1.0<\|y\|<2.0$	$2.0<\|y\|<3.0$
dN/dy per event	2.05	1.35	4.00	45.0

TABLE II

Summary of Detector Properties, Resolution and Limits

	Central ($\|y\|<2$)	Forward ($2<y<3$)
Absorber	$5\lambda_{abs}$ uranium	$6.7\lambda_{abs}$ aluminum
Muon Spectrometer	Iron toroids, prop. drift tube chambers	air-core toroids, prop. drift tube chambers, muon filter, TOF counters
m_T^{min}	3 GeV @ y = 0	0.4 GeV @ y = 3
$\frac{\Delta m_{\mu\mu}}{m_{\mu\mu}}$ ($p_T^{\mu\mu} \neq 0$)	20% @ 3 GeV, y = 0	40% @ 0.4 GeV, y = 3

VIII. COST ESTIMATE

An approximate cost estimate has been computed for the detector described above by scaling from the recently completed detailed cost estimate of the DØ Detector at Fermilab. The active absorber and drift tube/iron toroid system are quite similar to components of DØ. The air-core toroids are close to ones appearing in earlier versions of DØ, for which rough costs are known. The estimate is in FY85 dollars, exclusive of contigency and escalation:

ITEM	COST ($K)
Uranium Calorimeter (mech.)	1400
Aluminum Calorimeter (mech.)	350
Calorimeter Electronics (14k ch.)	700
Iron Toroids	500
Air-core Toroids	1000
Proportional Drift Tube Chambers	750
Chamber Electronics	400
Data Acq. (Trigger, Computers)	900
Cryogenics, Cables, Support	850
Installation, Administration	400
Detector Total	7250

Scaling the contingency from DØ (roughly 1/3) brings the cost close to $10M; escalating it to a 3 year construction period starting in, say, FY88 could bring the total to $12.5M in then-year dollars.

IX. SUGGESTIONS FOR EXTENDING THE PRESENT STUDY

Up to this point we have outlined the results of a "first cut" at the Problems of Dimuon Detection at RHIC. It appears feasible to carry such an effort through, but many details need to be explored. We list a few here.

A. Computation of Rate, Backgrounds and Acceptances.

It is necessary to improve the program described in Appendix 2 and to couple it directly to an event generator such as HIJET. Large statistics track-by-track studies of punchthrough and decay are needed to optimize the absorber. The segmentation of the absorber set down in Appendix I needs to be reviewed in the same context. The program needs to be extended to simulate the toroids and chambers as well as the absorber so that transverse mass resolution can be optimized. The effects of D^+D^- production on $\mu\mu$ backgrounds need to be included in background calculations.

B. Detector Details.

For purposes of definiteness and for easy computation of the cost estimate we took over detector design concepts wholesale from proton collider detectors. These all need further study. For example, the choice of a cryogenic absorber may cause problems in getting close to the beam. The use of aluminum in the forward spectrometer may not be optimum; other materials (for example boron carbide) have better ratios of χ_0/λ_0 and may be practical to use. The shape of the air toroids requires further optimization for acceptance, resolution, cost and power consumption.

C. Detector/Accelerator Interface.

We explored the impact of such a detector on RHIC (see Appendix 4). These questions need further study, because this detector places some special demands on the machine and because the design of both detector and machine are evolving. For example we require a small diameter beam pipe and can use high luminosity, however a very long luminous region will be difficult to exploit. These conflicting demands require some compromise which will have to come out of continued interaction with the machine designers and builders.

D. Other Physics.

We have not yet explored the range of physics problems that could be attacked with the detector. For example, at present the $|y| > 3$ at the region opposite to the forward spectrometer is uninstrumented. Studies of the baryon-rich region or of the fragmentation region could best be done here because of the global information available in the rest of the solid angle. We have tended to stress the trigger aspects of this information in conjunction with dimuons but should look at its ability to study the QGP in other events as well.

X. SUMMARY

A study of dimuon production in high energy nuclear collisions is a very elegant method for probing the formation of the quark-gluon plasma. Although about 4,000 hadrons are produced with heavy beams at top RHIC energies, a detector can be configured so that effectively only dimuons emerge from the (active) hadronic absorber.

We have shown that a suitable detector can be designed that will measure all the interesting values of m_T in the baryon free plateau. (There is no essential need to measure a given m_T over all values of y). This detector will have sufficient sensitivity to accurately resolve the resonances.

The cost of the detector will be fairly reasonable given the scale. Using known cost estimate from the DØ collaboration, we extrapolate a cost of $12.5M in then-year dollars including contingency.

Construction of such a detector for RHIC is imperative since dimuons continue to be a very promising probe of the quark-gluon plasma.

APPENDIX 1. ABSORBER INSTRUMENTATION

The absorber in the present design is active and provides global information about dimuon events for both triggering and analysis. Such a device is very similar to the segmented calorimeters used in high energy colliding beam detectors; there is much literature on this subject.[14]

The important features in the present case are: sufficient depth to contain hadron showers, short decay path between the interaction point and the absorber surface, and short interaction length. Segmentation of the active absorber may not be as fine as planned for future collider calorimeters such as DØ but will be qualitatively similar. Longitudinal segmentation allows discrimination between electromagnetic and hadronic energy deposition. Transverse segmentation allows measurement of energy flow, transverse energy, etc.

For the present study, and especially for the cost estimate, we have assumed a uranium-liquid argon absorber in the central region and an aluminum-liquid argon one in the forward region where the higher hadron momenta correspond to longer decay paths. The aluminum allows a lower multiple scattering limit on momentum resolution. Other materials, such as beryllium or boron carbide may be even better; more study is required. Readout techniques other than liquid argon are not ruled out although gas sampling probably dilutes the absorber too much in the central region. Again further study is needed to evaluate the trade-offs and select the best readout.

The towers are assumed to be $\Delta\phi = 0.1\ \pi \times \Delta z = 10$ cm $\times$ 5 depth segments, giving a total of 800 towers and 4000 readout channels. The 10 cm segmentation in z corresponds to $\Delta y = 0.5$ in the central region at a depth of about two absorption lengths. Equal-z segmentation was chosen because the long source length and the proximity of the absorber to the source preclude any useful equal-rapidity segmentation.

APPENDIX 2. ABSORBER MONTE CARLO

A very simple program was written to determine the survival probability of a pion or kaon after a spherical or cylindrical absorber. Three effects contributing to penetration of the absorber are considered: decay in flight

to muons, non-interacting punch-through and interacting punch-through. Absorber geometry, density, absorption length, and radiation length are specified at the start of a run. Hadron momentum and polar angle are also specified.

For each hadron the flight path for each of the three processes is calculated as described below. The minimum path is selected to determine the fate of each hadron. Energy loss by dE/dx is also computed along the path, so that particles range out in the absorber in some cases.

For decays, $\pi_{\mu 2}$ and $K_{\mu 2}$ modes were considered. Two-body kinematics is used to determine the muon momentum and direction from the decay point. From that point on its range is calculated to determine if it emerges from the absorber.

For non-interacting punch-through the survival probability is proportional to $\exp(-L/\lambda_0)$ where λ_0 is the absorption length.

For interacting punch-throughs the interaction point is also determined from the exponential above. From this point on the average number of charged particles in the shower is estimated by[15]

$$\bar{n} = 5\ E e^{-L/\lambda_{eff}}$$

where E is the interacting hadron's energy in GeV, L is the distance from the interaction point to the edge of the absorber, and λ_{eff} is given by

$$\lambda_{eff} = \lambda_0 E^{0.15}.$$

Given the average number, the probability that one or more survives for a given hadron is computed by Poisson statistics.

Figure 7 shows typical results from the program, plotted as the probability that a hadron of momentum p_{had} at rapidity y produces a "muon," i.e., a charged particle at the absorber edge. To compute the raw muon background rate these probability distributions were convoluted by hand with hadron spectra produced by HIJET.[16]

APPENDIX 3. IRON TOROIDS FOR RHIC DIMUON EXPERIMENT

Magnetic analysis of muon momenta in the region $|y| < 2$ is carried out with a system of toroidal iron magnets. The iron supplies additional material to absorb hadronic showers (7 λ_0 at y = 0, 10 λ_0 at $|y| = 2$). The transverse magnetic kick will be about 0.64 GeV/c at y = 0 and 0.92 GeV/c at $|y| = 2$. The muon toroids are divided into a central magnetized yoke, and forward and backward end-cap toroids.

Central

The central iron yokes will be assembled from 17 cm thick low carbon steel. There will be seven toroids each 2 m in length arranged concentrically so that the inner has an inside radius of 75 cm and the outermost has an outside radius of 215 cm. The inner toroid weighs 17 tons and the outer 40 tons; total weight for the central yoke is 200 tons.

The steel will be excited to 18 kG by copper coils. A relatively low current density design with water cooling has been chosen. The conductor has a square cross section of 1.6 in. × 1.6 in. with a cooling hole of 0.6 in. diameter. The design current is 2000 A.

Each of the seven concentric central toroids will be powered in series with 10 coils each of 20 turns for the outer toroid and 10 coils of 4 turns each for the inner toroid. Thus the increasing number of turns with radius will approximately establish a constant field strength of 18 kG. The parameters of the central coils are given in Table III.

End Cap

Each end-cap consists of ten iron toroids each 17 cm thick and outer radius of 215 cm. The inner radius varies with distance from the interaction point, corresponding to a polar angle of 15°; the toroid closest to (farthest from) the interaction point would have inner radius of 32 cm (80 cm). Each toroid weighs about 18 tons.

The end-cap toroids will be energized by 8 coils each containing 5 turns and with each common to all ten toroids. If these coils are constructed of the same conductor as used for the central toroids then a current of 2000 A should produce a field of 18 kG at a radius of 0.85 m falling off proportional to radius^{-1} for larger radii. These 40 turns (of 1.6 inch wide conductor)

completely fill the inside radius of the toroids at the front end (z = 1.2 m). Specific details of the end-cap windings are also given in Table III.

TABLE III

Iron Toroid Coils

	Central	End Cap
Current	2000 A.	2000 A.
Field	18 kG.	18 kG. ar r = 0.85 m.
Number of Coils	10	8
Turns in each Coil	4 to 10	5
Conductor Cross Section	1.60 × 1.60 $in.^2$	1.60 × 1.60 $in.^2$
Hole Diameter	0.60 in.	0.60 in.
Resistance of each Coil	2.3 mΩ	0.40 mΩ.
Total Resistance	23 mΩ	3.2 mΩ.
Total Voltage	46 V.	6.4 V.
Total Power	92 kW.	2 × 12.8 kW.
Total Length	2.2 km.	560 m (both end caps)

APPENDIX 4. AIR CORE TOROIDS FOR THE DIMUON EXPERIMENT AT RHIC

The double-toroid magnetic spectrometer placed downstream of the aluminum hadron absorber is designed to measure momenta and determine the sign of muons exiting the hadron absorber with momenta greater than 300 MeV/c. The hadron absorber is seven absorption lengths thick, corresponding to 703 g/cm^2 of aluminum and a kinetic energy threshold of ≈ 1.15 GeV for traversal by a muon. The toroids cover the range from pseudorapidity 2 (=15.4°) to 3 (=5.7°). It is expected that the central plateau formed in heavy-ion collisions at 100 GeV/A x 100 GeV/A will extend at least to $\Delta y = \pm 3$, with similar features over the full extent of the plateau. In particular, quark-gluon plasma characteristics deduced by observing dimuon pairs at y = 2-3 should be representative of the entire central plasma. This means one can study muon pairs with low transverse mass, even below 1 GeV/c^2,

by taking advantage of the large kinematic boost experienced by particles with y = 2-3 which allows muons forming a low invariant mass pair to penetrate the hadron absorber. The boost also improves mass resolution by decreasing multiple scattering in the hadron absorber. This is particularly important for a study of resonance production, especially for examining changes in positions or widths of resonances due to their "melting" at the phase transition.

The spectrometer is designed with the following criteria and constraints.

1. It must provide low enough $\int Bdl$ so as not to lose muons as soft as 300 MeV/c.
2. It should cause no further multiple scattering and therefore should be an air core toroid.
3. It should be able to cover up to $m_{\mu\mu} = 5$ GeV/c^2, and thus needs a large enough $\int Bdl$ to give reasonable resolution there.
4. It should allow space near the final machine beam-merging magnets, dipoles BC2, for insertion of special low β^* quadrupoles, as the dimuon cross sections are not expected to be large.
5. It should avoid introducing material into a cone with $\theta < 5^\circ$ with respect to the beam so as to avoid producing showers and resultant severe background from the very energetic hadrons in and near the projectile fragmentation region.
6. It must provide redundant tracking with high precision through the toroids, both for momentum resolution and sign determination and to reject hadron punch-through and shower punch-through particles.
7. It should incorporate a scintillator hodoscope trigger system that provides rough initial p_T information.
8. It should allow free space for inserting specialized central collision triggers, such as a device to trigger on the forward photons predicted by McLerran and Bjorken.
9. It should make a final check of muon/hadron rejection after the toroid(s) is(are) traversed.

10. It should maximize geometrical acceptance while minimizing power consumption, somewhat contradictory requirements for a copper coil air core toroid.

In addition, the hadron absorber must be active in order to include the measurement of $d^2E/dyd\phi$ for the range y = 2-3. The absorber needs to have the largest value feasible of χ_0/λ_0, radiation length divided by hadronic absorption length, to minimize the effect of multiple scattering on the mass resolution. Hadron absorbers made of, for example, Al, C, Be, B_4C, and LiH are being considered.

The device must be able to utilize a rather long luminous region due to the increase in beam bunch length due to intrabeam scattering for very heavy ions. Measures to counteract this by arranging for beam crossing at an angle are listed below.

It is proposed to meet the above requirements with the air core toroid spectrometer shown in Fig. 5. This would only be mounted on one side of the intersection point; the iron toroid part of the overall dimuon spectrometer and the central uranium absorber would be extended on the opposite side of the intersection region to cover the range $\theta < 15°$. The spectrometer incorporates (1) a pair of toroids with azimuthal magnetic fields $B_\phi(r)$ in opposing directions; (2) a number of drift chambers placed before, between, and after the toroids to provide tracking and position information for momentum determination; (3) a multilayer steel-drift chamber-hodoscope final absorber to provide a trigger and yet another layer of hadron rejection. It is also likely that hodoscopes will be included with the three sets of drift chambers next to the toroids to provide improved triggering and initial identification of roads through the toroids by taking advantage of the fact that a toroidal field does not change ϕ, the azimuthal angle, of a particle traversing its field.

Two toroids are used instead of one for the following reasons. Unlike spectrometers only looking at very energetic muons, where one strives to give the maximum feasible p_T kick to the muons in order to obtain a few mrad of deflection, the present system must handle muons ranging in momentum from 300 MeV/c to in excess of 15 GeV/c (e.g., a muon with m_T = 1.5 GeV/c^2 emitted

at y =3), a range of magnetic rigidity from 1 to 50 tesla-meters. An integrated $\int Bdl$ in a toroid of 0.5 Tm would give a 10-mrad kick to the latter muon but a 524-mrad (30°) deflection to the former. This would make it exceedingly difficult to measure the momentum of a 300-MeV/c muon, emitted at $\theta = 5°$ in the reaction, before it entered the region $|\theta| < 5°$ or passed through the collider beam pipe. Accordingly, the first toroid is arranged to provide a 5° deflection toward the beam pipe for a 300-MeV/c μ^- traveling initially at 6° (a 6° deflection to make the μ^- parallel to the axis would not be practical, as downstream detection elements would have to enter the "forbidden" $\theta < 5°$ cone), thus leaving a 300-MeV/c μ^+, which was initially emitted at 6°, traveling at 11° after the first toroid. After a meter or so of drift, the second toroid, with magnetic field opposite in direction to that in the first toroid, gives a much stronger kick to the muon pair (requiring 5.1 times the magnetic field as the first toroid), so that the μ^+ is bent toward the beam pipe so as to exit the third set of drift chambers just outside the $\theta = 5°$ cone.

It does not seem important to compensate the 1/r decrease of $B\phi$ in the first toroid, so its inner edge and both vertical sides are made rectangular; the outer edge is sloped at 18° to ensure that a 300-MeV/c μ^+ emitted at 16° exits the toroid on its downstream edge. The second toroid acts as the main momentum analyzer and thus has its upstream edge slanted to compensate the 1/r magnetic field fall-off. Its downstream edge is vertical for the following reasons. This allows mounting the downstream drift chamber both close to the toroid exit and radially with respect to the beam pipe, an advantage in construction. It also allows the soft, forward angle muons a longer drift space between two toroids than would be the case if the downstream edge of the toroid were slanted. This results in an increase in the allowed $\int Bdl$ of the second toroid, and thus in p_T kick for the hard muons, while still satisfying the constraint of keeping the $\theta < 5°$ cone clear.

We estimate that magnetic fields of $B_\phi(r) = 0.806$ kG/r[m] in the first toroid and $B_\phi(r) = 4.147$ kG/r[m] in the second are needed for the geometry shown in Fig. 5. The toroids' inner edges are 0.5 m long and are at radii of 46 cm and 52 cm.

A few options for winding the toroids from standard hard drawn copper were examined. A solution offering a reasonable compromise between transparency, power consumption, and coil extent along the beam axis is as follows. The toroids are wound from 2 cm x 2 cm copper conductor with a 6-mm central cooling hole. The windings are in the form of eight open center coils for each toroid. Parallel to the beam axis, on the inner radius, the coils are wound on a cylindrical inner support with each coil's windings spread out over 45° in azimuth to subtend as little polar angle as possible. On the vertical sides the coils are collected into a knife edge which is 3 turns wide in azimuth and extends parallel to the beam pipe as far as necessary (6 turns for the first toroid, 31 for the second). The outer radius just continues the vertical sections and is supported by a series of steel hoops.

The first toroid's transparency in azimuth is then found to be 83.3% at $\theta = 6°$, increasing linearly (with $\tan\theta$) to 93.9% at $\theta = 16°$. The $\int B \cdot dl$ is 0.174 T·m at $\theta = 6°$, falling to 0.0639 T·m at $\theta = 16°$, corresponding to p_T kicks of 52.2 MeV/c and 19.2 MeV/c, respectively. The inner cylindrical part of the coil subtends a polar angle of $\Delta\theta = 0.26°$, for example, from $\theta = 5.7°$ to 5.96°.

The first toroid is then found to need $4.03\ 10^5$ ampere-turns and is made of 8 coils of 18 turns each. This yields a current of 2797 amperes, a current density of 753 A/cm^2, a voltage to ground of 53.2 volts (all 8 coils in series) and a power consumption of 149 kW.

The second toroid's transparency in azimuth is found to be 85.2% at $\theta = 6°$, increasing linearly (with $\tan\theta$) to 96.3% at $\theta = 16°$. The $\int B \cdot dl$ is 0.399 T·m, on average at all angles from $\theta = 6°$ to 16°, corresponding to a p_T kick of 120 MeV/c. The inner cylindrical part of the coil subtends a polar angle of $\Delta\theta = 0.78°$, for example, from 5.2° to 5.98°.

The second toroid is found to need $2.07\ 10^6$ ampere-turns and is made of 8 coils of 93 turns each. This yields a current of 2782 amperes, a current density of 734 A/cm^2, a voltage to ground of 534 volts (all 8 coils in series), and a power consumption of 1.48 MW. These requirements can be met with conventional regulated DC supplies. At a power cost of $0.06/kwh and

2000 hour/year operation, assuming 50% transfer efficiency in power mains to toroid, an electrical power bill of about $400K/year to operate these magnets results.

The present design assumes that three sets each of drift chambers will be placed before the first toroid, between the two toroids and after the second toroid. These must be able to handle relatively large multiplicities which may reach mean values as high as 50 for Au + Au collisions at 100 x 100 GeV/nucleon. These multiplicities are comprised mostly of non-interacting punch-through hadrons from the primary event and punch-through products of hadron showers occuring in the hadron absorber. Due to these multiplicities, it appears quite useful to examine placing several thin (in terms of interaction lengths) chambers in each of the coil-free wedges in the two toroids in order to provide a large number of space points, of the order of fifty, for each track. This seems to be particularly necessary in view of the skewed tracks originating from hadron shower products emerging from the inner (5°) conical surface of the hadron absorber. These products are easily rejected if enough space points on their trajectory are available, as the trajectories will not exit from the downstream face of the hadron absorber.

The final downstream element in the spectrometer consists of a pair of scintillator hodoscopes, each segmented in θ and ϕ and placed one before and one after a 50-cm-thick iron absorber. Behind the second hodoscope is a last set of drift chambers. These hodoscopes act as primary triggers for the device, with the one in front of the iron tagging low momentum muons and the one behind it tagging muons with momenta greater than about 700 MeV/c, the minimum momentum for a muon to penetrate the iron. A third hodoscope just at the exit of the hadron absorber and a possible fourth between the two toroids are likely additions in order to provide time-of-flight information and provide information on roads through the device for the trigger hardware. It is also under consideration to segment the final iron into layers 17 cm (≈1 interaction length) thick and place chambers in the resulting gaps to observe any hadronic shower development. This would provide yet another level of hadron rejection against punch-through from the main hadron absorber into the toroid area.

Several areas for future study are apparent for the design of these toroids and associated chambers. They include:

1. A study, possibly using HIJET and the hadron shower code HETC, of the composition of the hadron showers in the hadron absorber as a function of number of absorption lengths traversed. Information on particle type, four-momenta, and point of exit from the hadron absorber is essential in order to perform reliable Monte Carlo studies of background events in the air core toroids and develop means of rejecting the same.
2. A study of the toroid optics, including the advantages and disadvantages of making the second toroid rectangular, except for the upper edge.
3. A study using open center vs. pancake vs. superconducting coils for the second toroid, both from a standpoint of optics and from that of power consumption vs. transparency.
4. A study of chamber and hodoscope segmentation to handle expected multiplicities, and a study of the tradeoffs in adding extra chambers in the toroid gaps to increase the number of space points on each particle's trajectory.

APPENDIX 5. BEAMS AT FINITE CROSSING ANGLE FOR THE DIMUON EXPERIMENT

The growth of rms bunch length in RHIC due to intrabeam scattering is especially severe for beams with $A \geq 100$. From Fig. IV.12 in the 1984 RHIC proposal, we see that after 2 hours, for Au + Au collisions at 100 x 100 GeV/nucleon, the rms bunch length grows to 110 cm, meaning the length of the luminous region for 95% of the events grows to $\sqrt{6}\ \sigma = 269$ cm. This is much larger than is feasible to handle, given the need of the dimuon experiment for a well-defined interaction point and small distances to hadron absorbers from the crossing point. Such a luminous region length would render it impossible to provide adequate hadron absorber depth for all possible crossing points without introducing unacceptably high, minimum muon energies required to penetrate the hadron absorber.

Accordingly, the possibility of having the beams cross at an angle will be considered in designing the experiment. This will decrease the length of the luminous region, but at the cost of decreasing the luminosity by the same factor. The relevant formulae are

$$L_\alpha = \frac{L_0}{\sqrt{1 + p^2}} \; ; \quad \sigma_{IR} = \frac{\sigma_\ell}{2\sqrt{1 + p^2}} ,$$

where

L_0 is the luminosity for 0° crossing,

L_α is the luminosity for crossing at α milliradians,

σ_ℓ is the rms bunch length (see Fig. IV.12, 1984 RHIC proposal),

σ_{IR} is the luminous region rms length,

$p = \alpha\sigma_\ell/2\sigma_H^*$.

α = crossing angle in milliradians

σ_H^* = horizontal rms bunch size at crossing point = $\sqrt{\varepsilon_N\beta_H^*/6\pi\beta\gamma}$

ε_N = normalized beam emittance = 10π mm mrad at 0 hours

18π mm mrad at 2 hours

28π mm mrad at 10 hours

β_H^* = lattice horizontal β function at crossing point; β_H^* = 3 m in standard lattice

β, γ are the usual Lorentz factors.

The following values result for crossing at 0, 2, 5, and 11 mrad for 0, 2, and 10 hours after a refill, Au + Au at 100 x 100 GeV/nucleon.

TABLE IV

α		mrad			
Time		0	2	5	11
0 hours $\varepsilon_N = 10\pi$	σ_ℓ(cm)	48	48	48	48
	σ_{IR}(cm)	24	9.8	4.2(2.5)	2.0
	$L(cm^{-2}s^{-1})$	$1.2\ 10^{27}$	$4.9\ 10^{26}$	$2.1\ 10^{26}$	$9.7\ 10^{25}$
2 hours $\varepsilon_N = 18\pi$	σ_ℓ(cm)	110	110	110	110
	σ_{IR}(cm)	55	13.9	5.7 (3.3)	2.6
	$L(cm^{-2}s^{-1})$	$6.7\ 10^{26}$	$1.7\ 10^{26}$	$7.0\ 10^{25}$	$3.2\ 10^{25}$
10 hours $\varepsilon_N = 28\pi$	σ_ℓ(cm)	148	148	148	148
	σ_{IR}(cm)	74	17.5	7.1 (4.2)	3.3
	$L(cm^{-2}s^{-1})$	$4.3\ 10^{26}$	$1.0\ 10^{25}$	$4.2\ 10^{25}$	$1.9\ 10^{25}$

The numbers in parentheses under 5 mrad are for $\beta^* = 1$ m, i.e., for a special low β^* insertion in the interaction region.

Thus it appears that a crossing angle of 5 mrad would provide a well-defined luminous region, even after 10 hours of Au + Au, of full length less than 35 cm, or less than 20 cm if arrangements can be made for special low β quadrupoles.

The luminosity penalty is not negligible, ranging from a factor 5 just after a refill to about 10 after 10 hours (due to the ever increasing bunch length), but is apparently a necessary price to ensure a well-defined interaction point.

Further study will focus on

a. possible size of crossing angles which can be accommodated to the lattice,

b. use of low β^* quads, which could make $\alpha = 2$ mrad attractive, with correspondingly high luminosity,

c. the possibility of stochastic cooling in RHIC to alleviate all the effects of intrabeam scattering.

For light ions, $A < 60$, where intrabeam scattering is not a problem, it appears that the head-on crossing mode is acceptable for the dimuon experiment, enabling full luminosity to be used.

REFERENCES

1. S. Chin, Phys. Lett. 119B, 51 (1982); G. Domokos and J. Goldman, Phys. Rev. D23, 203 (1981); K. Kajantie et al., Z. Phys. C9, 341 (1981); C14, 357 (1982); L. McLerran and T Toimela, Fermilab-Pub-84/84-T; R. Hwa and K. Kajantie, HU-TFT-85-2.
2. J. Bjorken and H. Weisberg, Phys. Rev. D13, 1405 (1976).
3. E. Shuryak, Phys. Lett. 78B, 150 (1978).
4. T. Goldman, et al., Phys. Rev. D20, 619 (1979).
5. K. Kinoshita, H. Satz, D. Schildknecht, Phys. Rev. D17, 17 (1978).
6. Data from I.R. Kenyon, Rep. Prog. Phys. 45, 1261 (1982).
7. M.G. Albrow, et al., Nucl. Phys. B155, 39 (1979).
8. Data from D. Drijard, et al., Zeit. Phys. C9 (1981).
9. G. Altarelli, et al., Phys. Lett. 151B, 457 (1985).
10. R. Pisarski, Phys. Lett. 110B, 155(1982).
11. J. Rafelski, Nucl. Phys. A418, 215C (1984).
12. A. Shor, Phys. Rev. Lett. 54, 1122 (1985).
13. J. Cleymans, et al., Phys. Lett. 147A, 186 (1984).
14. C.W. Fabjan and T. Ludlam, Annual Review of Nuclear and Particle Science 32, 335 (1982) and references cited therein.
15. DØ Design Report (December 1983), p. 139 (unpublished).
16. HIJET is a Monte Carlo event generator for relativistic nucleus-nucleus collisions based on ISAJET (T. Ludlam, unpublished).

FIGURE CAPTIONS

Fig. 1 Schematic of dimuons produced in a Quark Gluon Plasma.

Fig. 2 Schematic of conventional collider detector for dimuon study (note that this is not the preferred detector for RHIC).

Fig. 3 Calculations for dimuon rates in central collisions of Au + Au at $\sqrt{s}$ = 200 GeV/n assuming only conventional production (i.e. pp with appropriate scaling): a) $dN/dmdp_T^2$ for different masses at y = 2.5; b) Contours of equal dimuon rate versus $m_{\mu\mu}$ and y.

Fig. 4 Schematic of rapidity plateau of baryon free plasma and baryon rich regions.

Fig. 5 Dimuon detector for RHIC.

Fig. 6a Calculated mass resolution at $p_T = 0$ for dimuon spectrometer. Contours of equal percentage $m_{\mu\mu}$ resolution are plotted versus dimuon rapidity and mass.

Fig. 6b Expanded view of Fig. 6a in the region of low mass and large rapidity (i.e., the region accessible only to the air-core toroid system in the forward direction.)

Fig. 7 Probability that a hadron of momentum P_{had} at a given rapidity produces a "muon" for a cylindrical absorber arrangement.

Hadrons
QGP
Hadrons

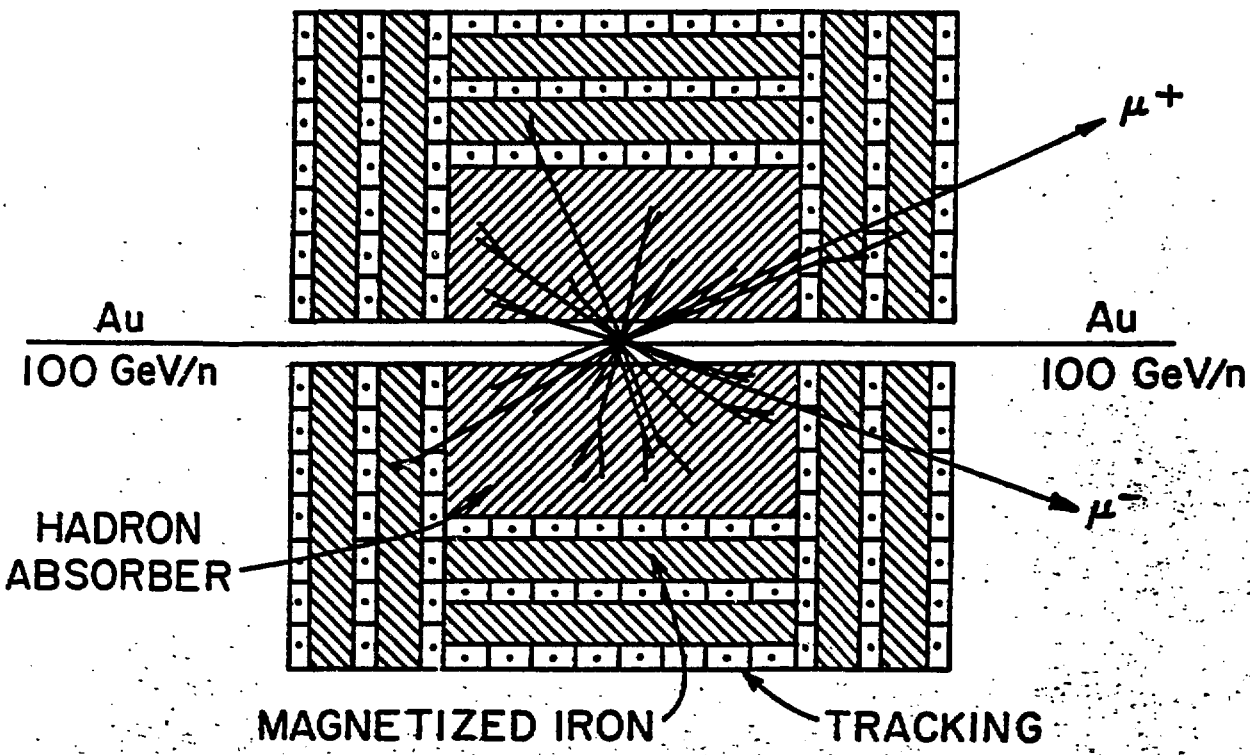
Au
100 GeV/n
Au
100 GeV/n
μ+
μ−
HADRON
ABSORBER
MAGNETIZED IRON
TRACKING

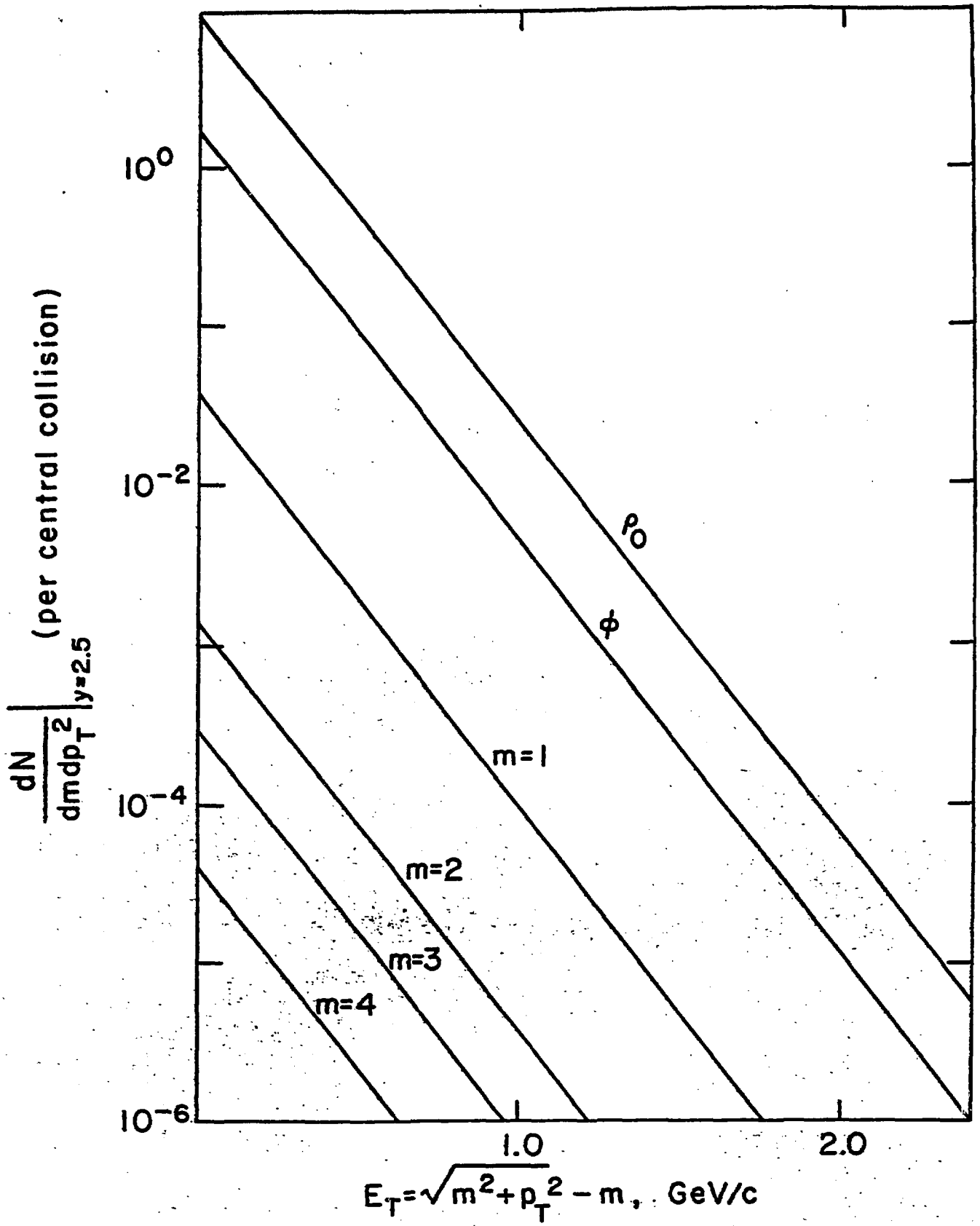
10^0
10^{-2}
10^{-4}
10^{-6}
$\frac{dN}{dm dp_T^2}\Big|_{y=2.5}$ (per central collision)
ρ_0
ϕ
m=1
m=2
m=3
m=4
1.0
2.0
$E_T = \sqrt{m^2 + p_T^2} - m$, GeV/c

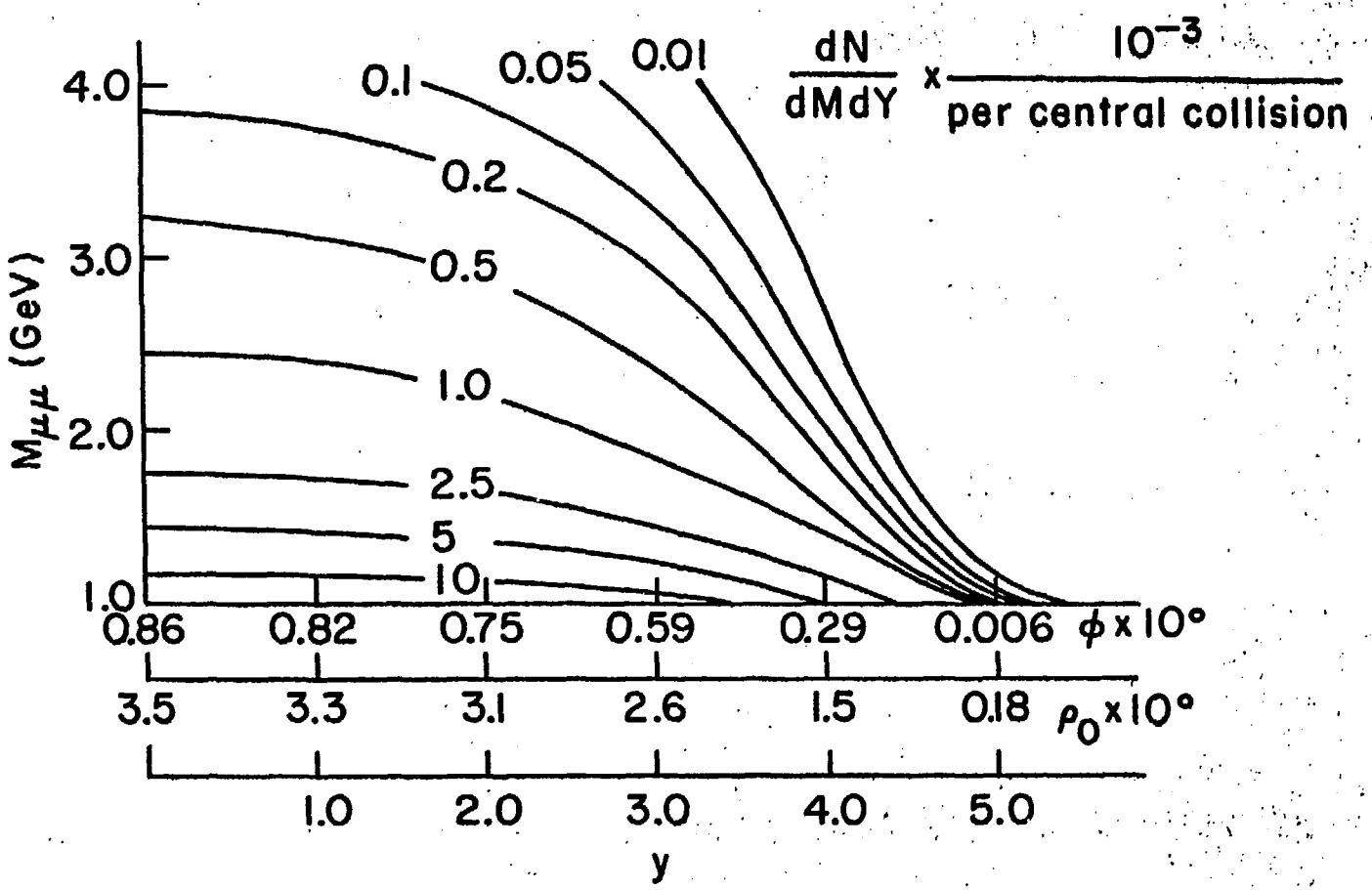
4.0
3.0
2.0
1.0
$M_{\mu\mu}$ (GeV)
0.1
0.05
0.01
0.2
0.5
1.0
2.5
5
10
$\frac{dN}{dMdY} \times \frac{10^{-3}}{\text{per central collision}}$
0.86
0.82
0.75
0.59
0.29
0.006
$\phi \times 10^{\circ}$
3.5
3.3
3.1
2.6
1.5
0.18
$\rho_0 \times 10^{\circ}$
1.0
2.0
3.0
4.0
5.0
y

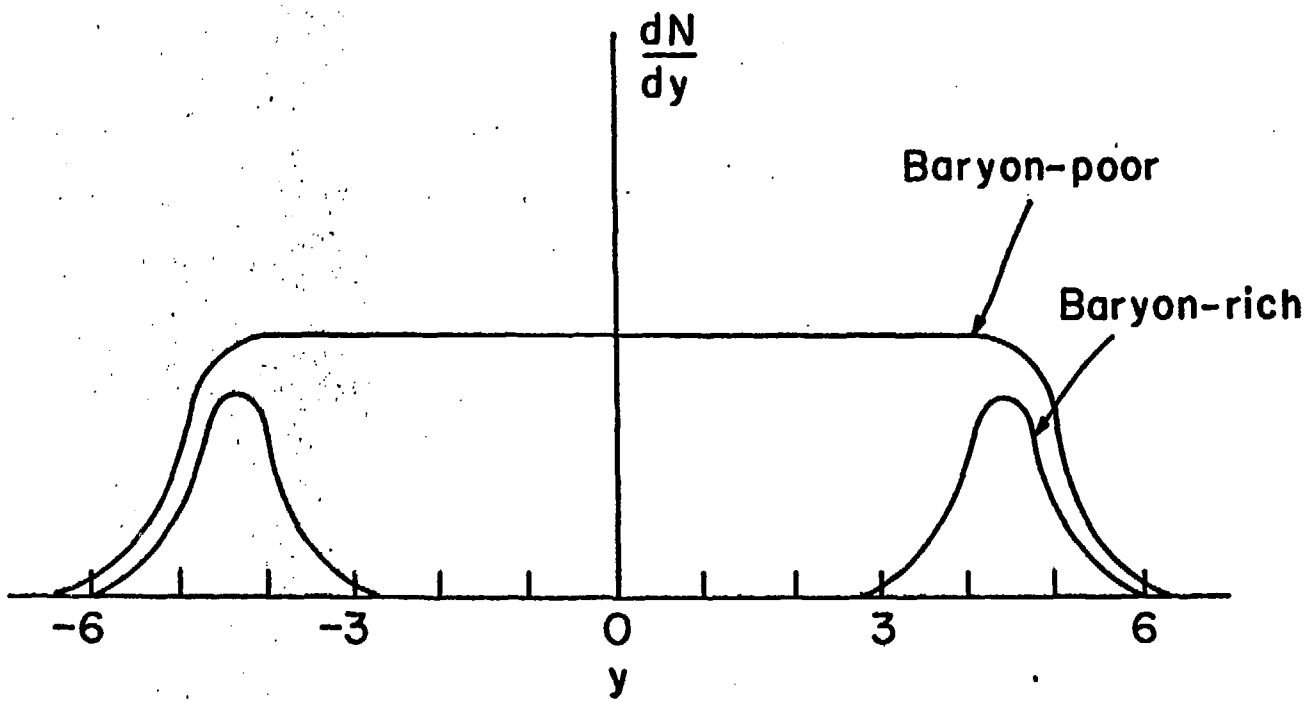
dN
dy
Baryon-poor
Baryon-rich
-6
-3
0
3
6
y

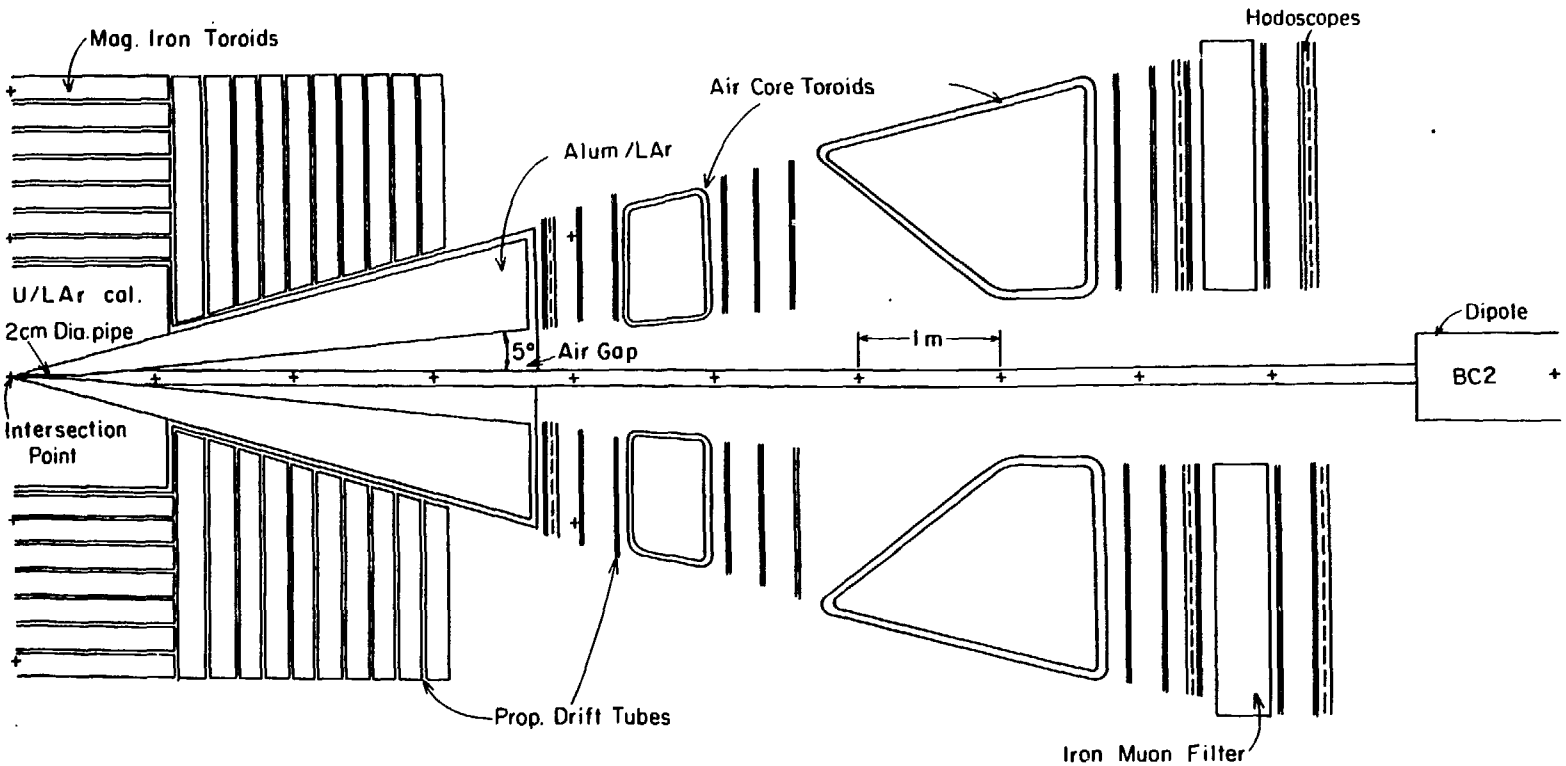
Mag. Iron Toroids
Hodoscopes
Air Core Toroids
Alum /LAr
U/LAr cal.
2cm Dia. pipe
5°
Air Gap
1 m
Dipole
BC2
Intersection Point
Prop. Drift Tubes
Iron Muon Filter

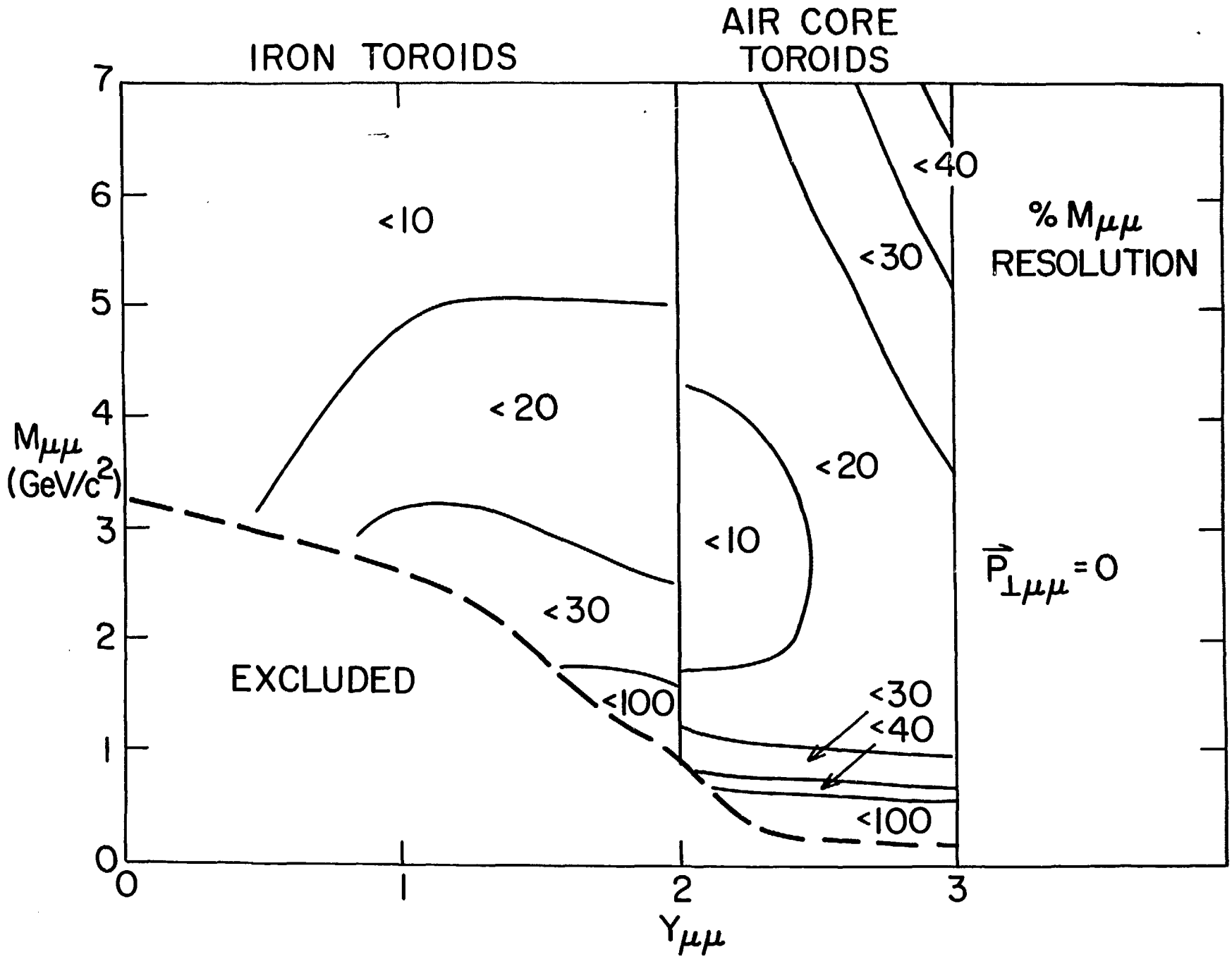
IRON TOROIDS
AIR CORE TOROIDS
% Mμμ RESOLUTION
<10
<20
<30
<40
<100
<10
<20
<30
<30
<40
<100
EXCLUDED
$\vec{P}_{\perp\mu\mu}=0$
Mμμ (GeV/c²)
Yμμ
0
1
2
3
0
1
2
3
4
5
6
7

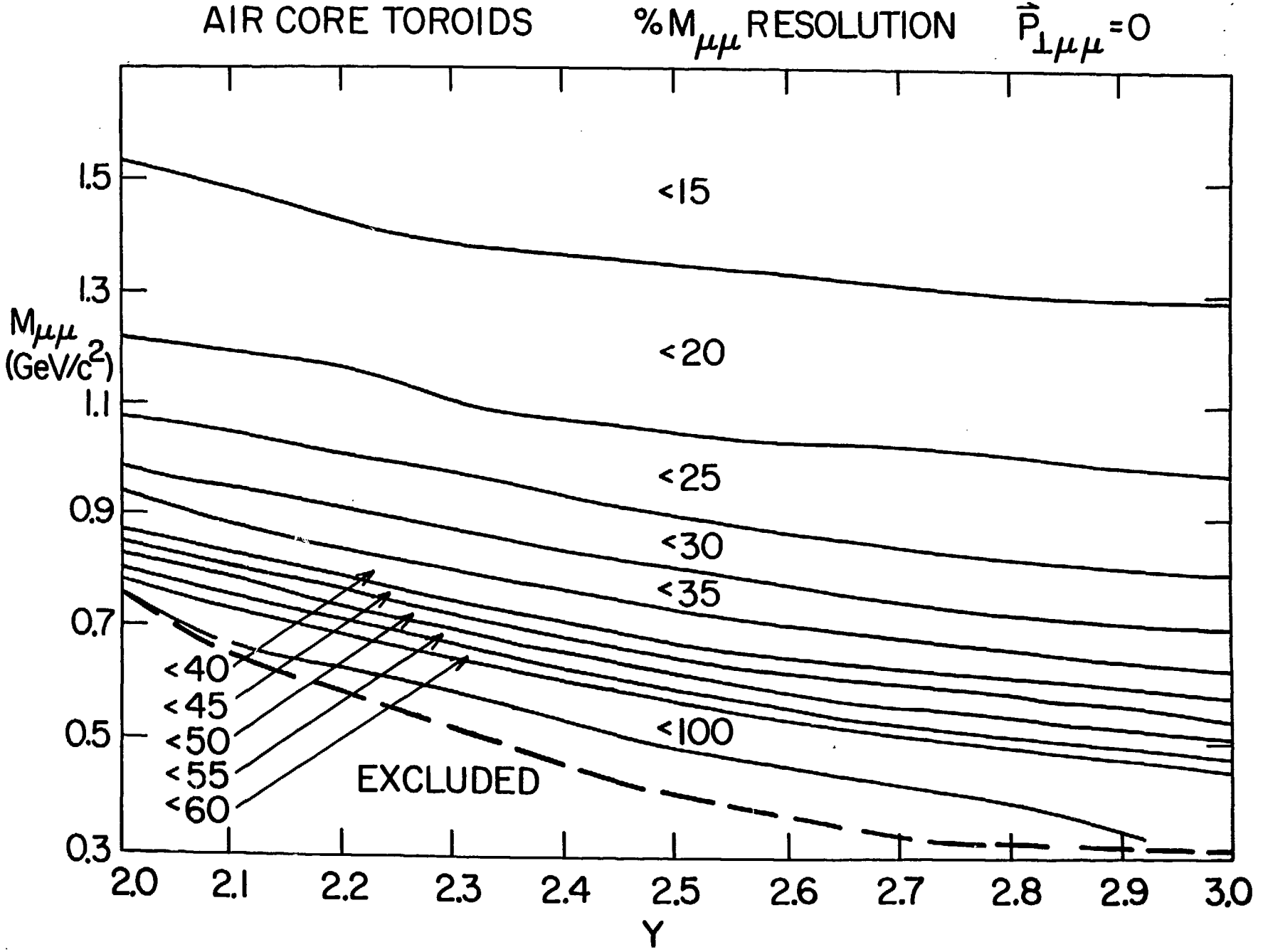
AIR CORE TOROIDS
%$M_{\mu\mu}$ RESOLUTION
$\vec{P}_{\perp\mu\mu}=0$
<15
<20
<25
<30
<35
<40
<45
<50
<55
<60
<100
EXCLUDED
$M_{\mu\mu}$ (GeV/c^2)
1.5
1.3
1.1
0.9
0.7
0.5
0.3
2.0
2.1
2.2
2.3
2.4
2.5
2.6
2.7
2.8
2.9
3.0
Y

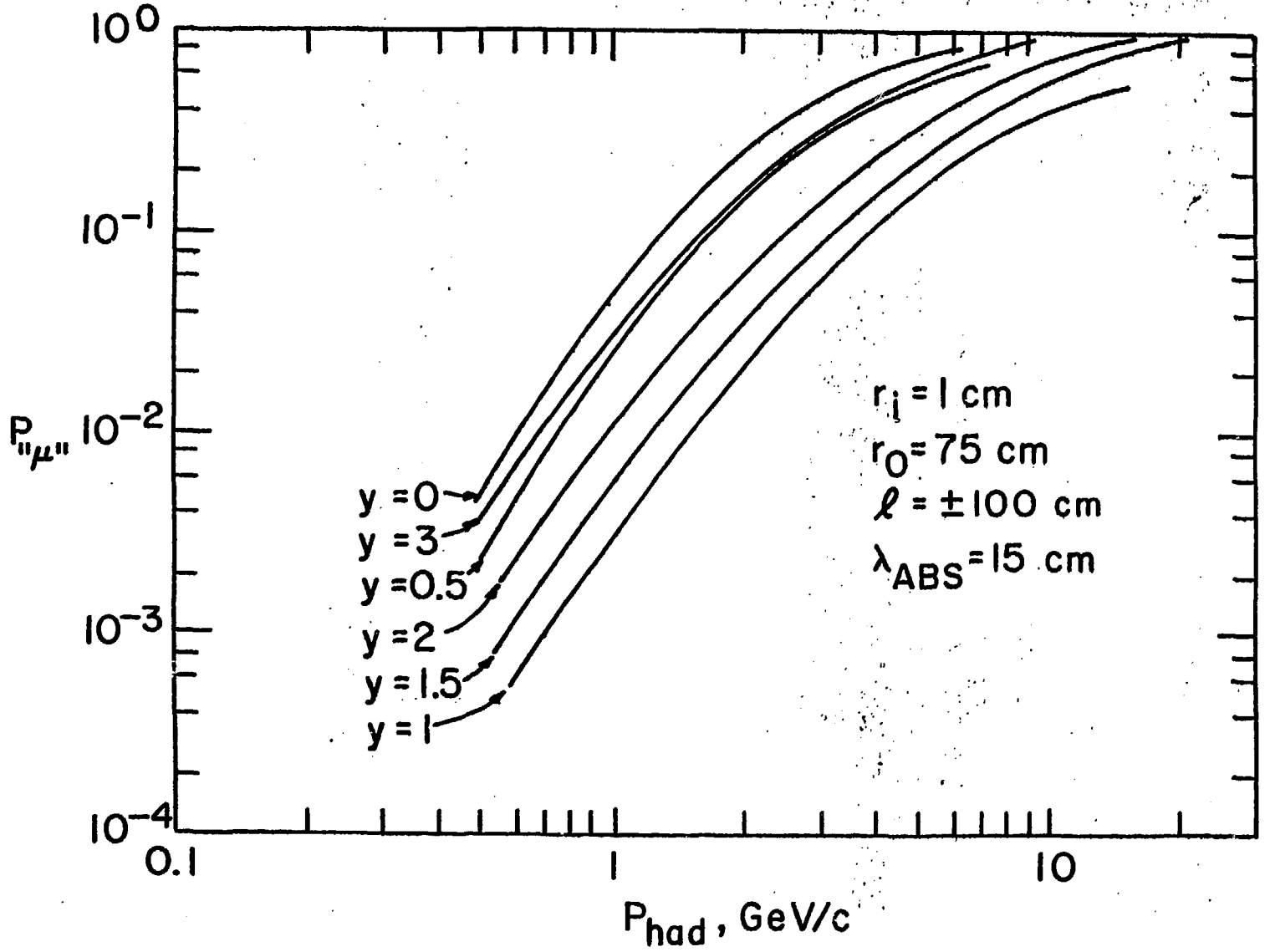
10^0
10^{-1}
10^{-2}
10^{-3}
10^{-4}
$P_{"\mu"}$
0.1
1
10
P_{had}, GeV/c
y = 0
y = 3
y = 0.5
y = 2
y = 1.5
y = 1
r_i = 1 cm
r_o = 75 cm
ℓ = ±100 cm
λ_{ABS} = 15 cm